International Journal of Biological Macromolecules 126 (2019) 376–384

Contents lists available at ScienceDirect

International Journal of Biological Macromolecules

journal homepage: http://www.elsevier.com/locate/ijbiomac

Structural characterization of lignin and its carbohydrate complexes isolated from bamboo (*Dendrocalamus sinicus*)

Gaofeng Xu [a,b], Zhengjun Shi [a,b,*], Yihe Zhao [c], Jia Deng [a], Mengyao Dong [d,e,f], Chuntai Liu [e,f], Vignesh Murugadoss [d], Xianmin Mai [g], Zhanhu Guo [d,**]

[a] Key Laboratory for Forest Resources Conservation and Utilization in the Southwest Mountains of China, Ministry of Education, Southwest Forestry University, Kunming 650224, China
[b] College of Chemical Engineering, Southwest Forestry University, Kunming 650224, China
[c] Yunnan Academy of Forestry, Kunming 650224, China
[d] Integrated Composites Laboratory (ICL), Department of Chemical and Biomolecular Engineering, University of Tennessee, 322, Dougherty Engineering Bldg., Knoxville, USA
[e] Key Laboratory of Materials Processing and Mold, Zhengzhou University, Ministry of Education, Zhengzhou 450002, China
[f] National Engineering Research Center for Advanced Polymer Processing Technology, Zhengzhou University, Zhengzhou 450002, China
[g] School of Urban Planning and Architecture, Southwest Minzu University, Chengdu 610041, China

ARTICLE INFO

Article history:
Received 7 November 2018
Received in revised form 24 December 2018
Accepted 24 December 2018
Available online 26 December 2018

Keywords:
Organosolv lignin
Lignin-carbohydrate complex
Isolation
Structural characterization

ABSTRACT

Isolation of earth abundant biopolymer, Lignin, from *Dendrocalamus sinicus* and their structural properties were investigated to achieve its large-scale practical applications in value-added products. Two lignin fractions (MWL, DSL) were isolated with successive treatments of dioxane and dimethylsulfoxide (DMSO) from dewaxed and ball milled bamboo (*D. sinicus*) sample. The two-step treatments yielded 52.1% lignin based on the total lignin content in the dewaxed bamboo sample. Spectroscopy analyses indicated that the isolated bamboo lignin was a typical grass lignin, consisting of *p*-hydroxyphenyl, guaiacyl, and syringyl units. The major interunit linkages presented in the obtained bamboo lignin were *β*-*O*-4′ aryl ether linkages, together with lower amounts of *β*-*β*′, *β*-5′, and *β*-1′ linkages. The tricin was detected to be linked to lignin polymer through the *β*-*O*-4′ linkage in the bamboo. In addition, phenyl glycoside and benzyl ether lignin-carbohydrate complexes (LCC) linkages were clearly detected in bamboo (*D. sinicus*), whereas the *γ*-ester LCC linkages were ambiguous due to the overlapping NMR signals with other substructures. The detailed structural properties of the obtained lignin fraction together with the light-weight will benefit efficient utilization of natural polymers as a possibly large-scale bio-based precursor for making polymeric materials, biochemicals, functional carbon and biofuels, and multifunctional polymer nanocomposites.

1. Introduction

Polymer based materials have attracted great attention both in industry and academia because of their remarkable properties and low cost. However, the serious environmental problems due to the non-biodegradable polymers from petroleum industry have demanded the exploration of biopolymers. Among various bio-polymers, lignin is second abundant bio-polymer in the earth [1,2], that can potentially contribute to a wide range of value added products such as membranes, foams, carbon materials, engineered plastics, bio-based composites, liquid fuels and commodity chemicals [3]. Although researchers have reported lignin for more than a century, due to its complex structure, its effective usage is limited to only 2% [4,5]. Therefore, it is necessary to make progress in analytical chemistry, detailing the structure of lignin to achieve its large-scale applications. In this work, we investigated the structural properties of lignin derived from *Dendrocalamus sinicus*.

Bamboo, *Dendrocalamus sinicus*, the world's largest bamboo species, belonging to *Bambusoideae* of *Gramineae*, with strong woody stems (maximal diameter 30 cm, maximal height 33 m), is mainly distributed in the southwest region of China [6]. Traditionally, as raw materials, this kind of bamboo species is widely used in construction, paper making, and man-made board industries. Due to its easy propagation, fast growth, and high productivity, *D. sinicus* is considered as one of the most potential renewable non-woody forestry feedstock for lignocellulosic biorefinery. Given the growing interest in bamboo as feedstock for bio-chemicals and biomaterials, it is important to understand the composition and structure of components in the cell wall of the bamboo stem in order to effectively utilize it as a precursor to biomaterials or green chemicals.

* Correspondence to: Z.J. Shi, Key Laboratory for Forest Resources Conservation and Utilization in the Southwest Mountains of China, Ministry of Education, Southwest Forestry University, Kunming 650224, China.
** Corresponding author.
E-mail addresses: shizhengjun1979@163.com (Z. Shi), zguo10@utk.edu (Z. Guo).

https://doi.org/10.1016/j.ijbiomac.2018.12.234
0141-8130/

Compared with the other natural components (cellulose and hemicelluloses), lignin is an extremely complex three-dimensional polymer (typically found in vascular plants) formed by dehydrogenative polymerization of *p*-hydroxycinnamyl, coniferyl, and sinapyl alcohols. These three lignin precursors ('monolignols') give rise to the so-called *p*-hydroxyphenyl (H), guaiacyl (G), and syringyl (S) phenylpropanoid units, which show different abundances in lignin from different groups of vascular plants, as well as in different plant tissues and cell-wall layers [3]. Unlike most natural polymers, which consist of a single intermonomeric linkage, lignin is an amorphous, three-dimensional copolymer of phenylpropanoid units linked through ether and carbon carbon bonds such as *β*-*O*-4′, 4-*O*-5′, *β*-*β*′, *β*-1′, *β*-5, and 5–5′ [7].

Besides these 20 different types of bonds present within the lignin itself, lignin is covalently linked to hemicellulosic polysaccharides, hindering the effective separation of the wood components and the efficiency of enzymatic hydrolysis of carbohydrates [8,9]. It was generally accepted that benzyl-ether and phenyl-glycoside linkages are the main bonds of lignin-carbohydrate complexes (LCC) in hardwood and softwood. On the other hand, ferulate and *p*-coumarate link both hemicelluloses (mainly arabinoxylan) and lignin together by benzyl-ester forming LCC in the herbaceous [10]. The term "lignin-carbohydrates complex" was first used by Björkman to describe the preparation of hemicelluloses accompanied by lignin, and many isolation procedures have been proposed to prepare LCC [11]. Among the reported methods, solvent extraction from various untreated plant cell walls under mild conditions is the most common and effective method, because any chemical or biochemical treatment before LCC isolation would break the possible linkages between lignin and carbohydrates [12]. However, it has been extremely difficult to obtain unambiguous evidence on the nature and frequency of such linkages in the real plants [13]. Therefore, it is vitally important to understand the structure of native lignin and LCC in the lignocellulosic biomass.

Understanding the specific structural characteristics of lignin is conducive to develop an efficient and economical conversion technology for lignocellulosic resource biorefinery. The aim of the present study was to investigate the structural characteristics and physicochemical properties of lignin and LCC subfractions present in *D. sinicus*. In this study, the bamboo materials were sequentially treated with dioxane and DMSO. The obtained lignin preparations were characterized by Fourier transform infrared spectroscopy (FT-IR), gel permeation chromatography (GPC), high-performance anion exchange chromatography (HPAEC), and 2D heteronuclear single quantum coherence magnetic resonance (2D HSQC NMR) spectroscopy.

2. Experimental work

2.1. Materials

Bamboo (*D. sinicus*) sample (Fig. S1), 3 years old, was collected from Yunnan Province, China. It was first dried in oven at 60 °C and then chipped into small pieces. The oven-dried bamboo samples were ground and screened to obtain a 40–60 mesh powder. This bamboo fraction was subjected to extraction with toluene/ethanol (2:1, v/v) in a Soxhlet apparatus for 6 h to remove max. The extractive-free bamboo sample contained 44.50% cellulose, 28.6% lignin (25.0% Klason lignin, 3.6% acid-soluble lignin), and 17.6% hemicelluloses, determined according to National Renewable Energy Laboratory's standard analytical method [14]. The dewaxed 40–60 mesh bamboo powder was milled in a planetary ball mill (Fritsch, Germany) equipped with a 500 mL ZrO_2 bowl containing mixed balls (10 balls of 2 cm diameter and 25 balls of 1 cm diameter). The milling was conducted for 5 h (a 10 min lull after every 10 min of milling) under a nitrogen atmosphere at 450 rpm. All standard chemicals, such as monosaccharide and chromatographic reagents, were analytical or reagent grade without further purification.

Table 1
Yields and carbohydrate contents of lignin fractions isolated from the dewaxed *D. sinicus*.

Lignin	Yield (%)	Purity (%)	Polysaccharides (%)	Monosaccharide (%)					
				Rha	Ara	Gal	Glu	Xyl	Glca
MWL	6.1	81.5	16.2	ND	3.2	ND	10.9	84.7	1.2
DSL	8.8	87.6	9.7	ND	2.1	ND	8.4	89.5	ND

Abbreviations: Rha, rhamnose; Ara, arabinose; Gal, galactose; Glu, glucose; Xyl, xylose; Glca, glucuronic acid; N.D, not detectable.

Table 2
Weight-average (M_w) number-average (M_n) molecular weights and polydispersity (M_w/M_n) of the lignin fractions isolated from *D. sinicus*.

	Lignin fractions	
	MWL	DSL
M_w	4650	3760
M_n	2840	2090
M_w/M_n	1.6	1.8

2.2. Isolation of lignin fractions

A scheme for separation of bamboo (*D. sinicus*) lignin was shown in Fig. S2. The procedures are illustrated as follow: The dewaxed and ball milled bamboo sample was firstly suspended in 96% dioxane with a solid-to-liquid ratio of 1:20 (g/mL) at room temperature for 48 h to isolate mill wood lignin (MWL) according to the method of Björkman [15]. The extraction procedure was conducted in the dark and under a nitrogen atmosphere. After extraction, the mixture was filtered and the residue was washed with the same solvents until the filtrate was clear. The purification procedure was according to the method of Sun [16]. The combined filtrates were first concentrated with a rotary evaporator under reduced pressure and then precipitated in 3 volumes of 95% ethanol to precipitate hemicelluloses. A pellet rich in hemicelluloses was recovered by filtering, washing with 70% ethanol, and freeze-drying. After evaporation of ethanol, the 96% dioxane soluble lignin (MWL) was obtained by precipitation in acidic condition, which was adjusted to pH 1.5–2.0 by 6 M HCl. The residue free of 96% dioxane-soluble was successively treated with 95% DMSO at 85 °C for 5 h with a solid-to-liquid ratio was 1:20 (g/mL). The DMSO-soluble lignin fraction (DSL) was obtained according to the same method as precipitation of MWL before freeze-drying. All the experiments were performed at least in duplicate. The relative standard deviation was observed to be lower than 4.8%. Yields of the lignin fractions were calculated on dry weight basis related to the dewaxed bamboo samples.

2.3. Characterization of lignin fractions

The hemicellulosic moieties associated with the lignin fractions were determined by hydrolysis with dilute sulfuric acid according to the method suggested by Sun [17]. That is, 4–6 mg sample of lignin was hydrolyzed with 1.475 mL of 6.1% H_2SO_4 for 2.5 h at 105 °C. After hydrolysis, the mixture was filtered, and the filtrate containing the liberated neutral sugars was analyzed by high-performance anion exchange chromatography (HPAEC) system (Dionex ICS 3000, U.S.) with pulsed amperometric detector and an ion exchange Carbopac PA-1 column (4 × 250 mm). Neutral sugars were separated in 18 mM NaOH (carbonate free and purged with nitrogen) with postcolumn addition of 0.3 M NaOH at a rate of 0.5 mL min^{-1}. Run time was 45 min, followed by 10 min elution with 0.2 M NaOH to wash the column and then a 15 min elution with 18 mM NaOH to reequilibrate the column. Calibration was performed with standard solutions of L-rhamnose, L-arabinose, D-glucose, D-galactose, D-mannose, D-xylose, glucuronic acid, and galacturonic acid. The analyses were run twice, and the average values were calculated for all of the lignin fractions.

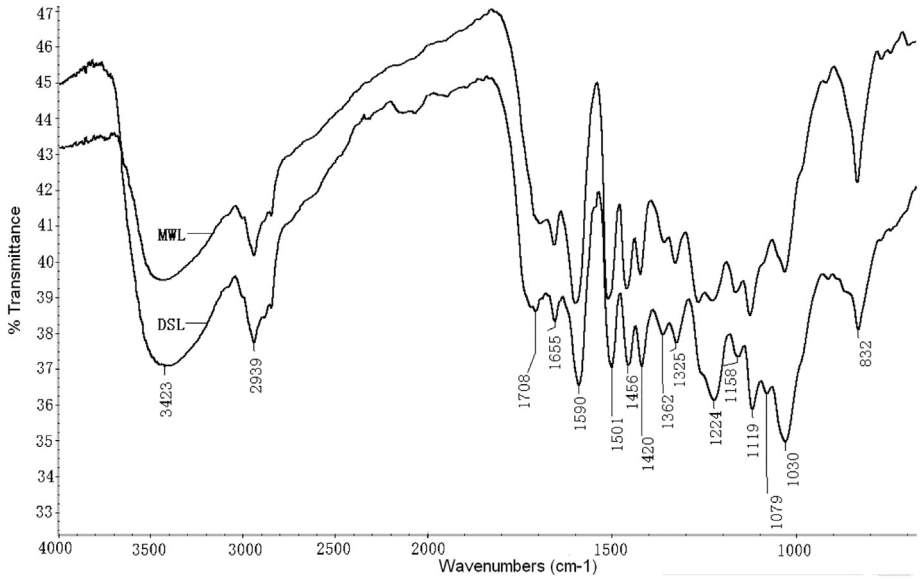

Fig. 1. FT-IR spectra of lignin fractions isolated from *D. sinicus*.

The weight-average (M_w) and number-average (M_n) molecular weights of the lignin fractions were determined by GPC (Agilent 1200, USA) with a refraction index detector on a PL-gel 10 μm Mixed-B 7.5 mm ID column, calibrated with PL polystyrene standards. 4 mg lignin sample was dissolved in 2 mL tetrahydrofuran, and 20 μL sample in solution was injected. The column was operated at ambient temperature and eluted with tetrahydrofuran at a flow rate of 1.0 mL min^{-1}.

FT-IR spectra of lignin fractions were conducted using a Thermo Scientific Nicolet iN10 FT-IR Microscope (Thermo Nicolet Corporation, Madison, WI, USA) equipped with a liquid nitrogen cooled MCT detector. The dried samples were ground and palletized using BaF_2, and their spectra were recorded in the range from 4000 to 700 cm^{-1} at 4 cm^{-1} resolution and 128 scans per sample. The fingerprint region was baseline corrected between 1900 and 750 cm^{-1}. Before data collection, a background scanning was performed for background correction.

NMR spectra were recorded with a Bruker AVIII 400 MHz spectrometer according to our former published reports [18]. The 2D HSQC spectra were acquired in the HSQC GE experiment mode. The spectral widths were 1800 Hz and 10,000 Hz for the ^{1}H- and ^{13}C-dimensions, respectively. A 128 scanning time, a 2.6 s delay time between transients, and a 1.5 s relaxation time were used. The $^1J_{C\text{-}H}$ used was 145 Hz. The central solvent (DMSO) peak was used as an internal chemical shift reference point (δ_C 39.5; δ_H 2.49 ppm). Prior to Fourier transformation, the data matrixes were zero filled up to 1024 points in the ^{13}C-dimension. Data processing was performed using standard Bruker Topspin NMR software.

3. Results and discussion

3.1. Yield and carbohydrate composition

In the plant cell walls, lignin is associated with cellulose and hemicelluloses by hydrogen bonds and covalent bonds (mainly ether and ester linkages), respectively. Therefore, isolation of lignin in a pure form from plant cell walls involves hydrolysis of ester and ether linkages followed by extraction them into aqueous media [19]. As shown in Table 1, the successive treatments of the dewaxed bamboo sample with dioxane and DMSO resulted in a dissolution of 6.1 and 8.8% of the bamboo lignin fractions (percent of the dry starting material), respectively.

To precisely evaluate the efficiency of the two-step sequential treatments on bamboo lignin solubilization, the lignin content in the isolated lignin fractions was determined by the standard methods [14]. As shown in the Table 1, the lignin content (including acid soluble lignin and acid insoluble lignin) for MWL and DSL was 81.5% and 87.6%, respectively. Based on the purity analysis results, it could be speculated that 44.3% original lignin (percent of original lignin in bamboo) was obtained after the two-step treatments in the present study.

The composition of the associated hemicelluloses in the isolated lignin fractions were determined by their contents of neutral sugars and uronic acids, and the analytical results are also listed in Table 1. Clearly, both MWL and DSL contained considerable amounts of bound polysaccharides as shown by the neutral sugar and uronic acid contents. This result revealed that the sequential treatments with dioxane and DMSO under the conditions used did not significantly cleave the LCC bonds between lignin and polysaccharides in the cell wall of bamboo. The MWL and DSL fractions contained a large percentage of xylose among the total sugars and uronic acids. In other words, xylose was the predominant sugar composition among the five kinds of sugars and uronic acids. These results suggested that xylans in the plant wall were the predominant hemicelluloses which crossly linked with lignin. Other sugars, such as glucose and arabinose, were also observed in noticeable amounts.

3.2. Molecular weight

In order to investigate the molecular weights of the lignin fractions sequentially extracted with dioxane and DMSO solutions, weight-average (M_w) and number-average (M_n) molecular weights, as well as the polydispersity (M_w/M_n) of the of MWL and DSL were determined by GPC and the results are given in Table 2. As can be seen, MWL and DSL exhibited unlike weight-average molecular weights, 4650 and 3760 g mol^{-1}, respectively. The weight-average molecular weight of MWL was slightly higher than that of DSL. It has been documented that the carbohydrate chains linked to lignin can increase the hydrodynamic volume of lignin, thus increasing the apparent molar mass of lignin in GPC measurements [20]. Therefore, the relative higher molecular weights of MWL may result from its higher carbohydrate contents than that of DSL as shown in Table 1. In addition, both MWL and DSL exhibited relatively narrow molecular weight distributions, as shown by $M_w/M_n < 1.80$. Polydispersity is an important parameter of natural

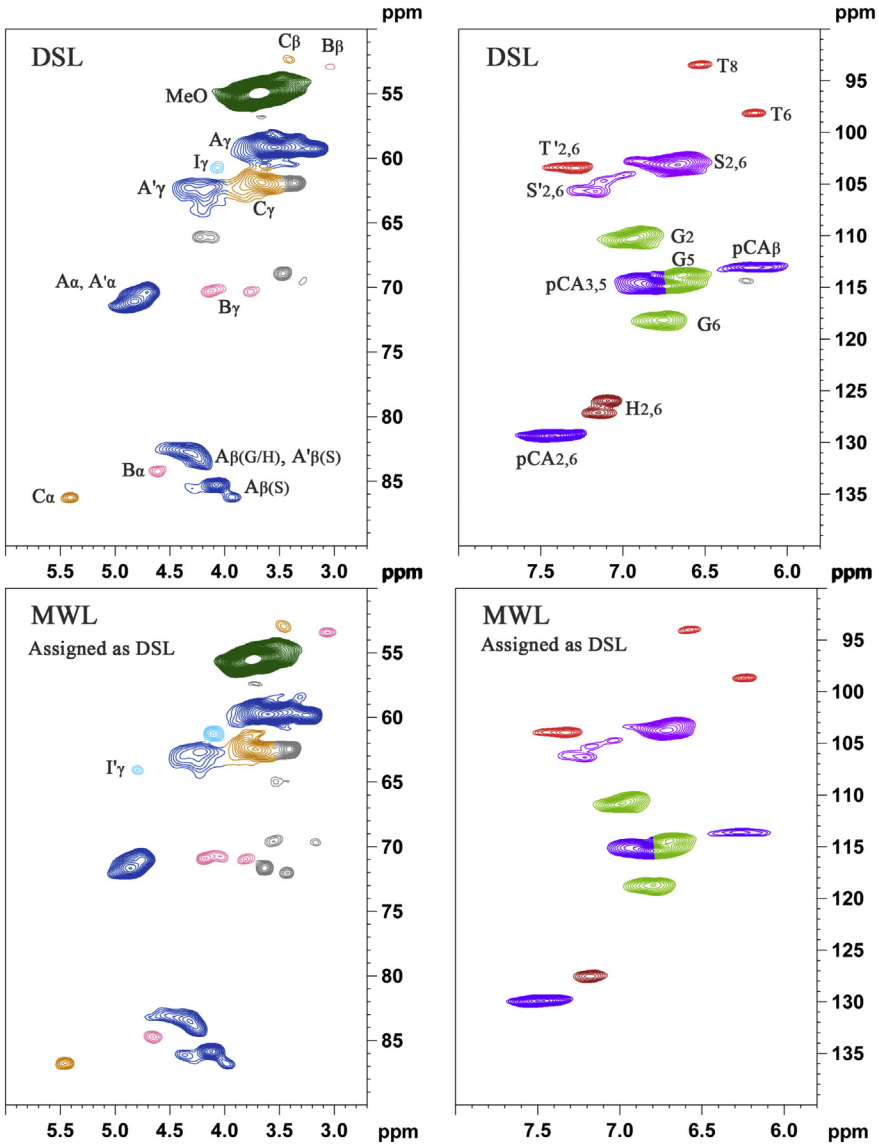

Fig. 2. HSQC-NMR spectra of lignin fractions (MWL and DSL) isolated from *D. sinicus*.

macromolecules relative to their applications in process of biorefinery. In general, a narrower polydispersity means a better physicochemical stability. From this point of view, it is important to obtain lignin polymers with a relatively narrow polydispersity from plants resources.

3.3. FT-IR analysis

Fig. 1 shows the FT-IR spectra of MWL and DSL isolated from bamboo (*D. sinicus*). The FT-IR spectra have been recorded and the peaks were assigned by comparing their wavenumbers with previous literatures [21–23]. An analogous structure of the lignin fractions can be seen from Fig. 3, because the spectra of MWL and DSL showed minor changes in the peaks and the absorption intensities. Obviously, a wide absorption band focused at 3423 cm^{-1} is attributed to OH stretch, and bands at 2924 and 2939 cm^{-1} are assigned to CH stretch in CH_2 and CH_3 groups, respectively. The presence of the unconjugated carbonyl stretch at 1708 cm^{-1} in MWL and DSL indicate that the ester groups between lignin and hemicelluloses were remained during the treatments of dioxane and DMSO, which corresponded to the results of lignin purity analysis in Table 1. The band at 1655 cm^{-1} is attributed to conjugated carbonyl stretching in lignin. The aromatic skeleton vibration in the lignin fractions occurs at 1590, 1501, and 1420 cm^{-1}. Absorption of 1456 cm^{-1} indicates the methoxyl C—H deformation and aromatic ring vibration. The weak band at 1362 cm^{-1} arises from the aliphatic C—H stretch in CH_3. The 1325 and 1224 cm^{-1} bands are assigned to syringyl and guaiacyl ring breathing, respectively. The bands at 1119 cm^{-1}, 832 cm^{-1}, and shoulder at 1158 cm^{-1} in lignin indicate a typical structure of lignin with *p*-hydroxy phenylpropane (H), guaiacyl (G), and syringyl (S) units. Similar results were also found in the NaOH extracted bamboo lignin from *Bambusa rigida species* and *Pyllostachys makinoi* Hay [24,25].

3.4. 2D-HSQC NMR analysis

Two-dimensional ^{1}H-^{13}C NMR (2D NMR) spectroscopy can provide important compositional and structural information of the lignin and LCC [26]. In addition, the application of 2D HSQC NMR can also provide a direct evidence of the structural characteristics and the linkages of LCCs [8]. The 2D-HSQC NMR spectra of the lignin and LCC in the isolated bamboo lignin fractions are shown in Figs. 2 and 5, respectively. The main substructures of bamboo lignin and LCC linkages are depicted in Figs. 3 and 4, respectively. The HSQC crossing signals of lignin and LCC are assigned by the published literature [9,27–30]. The assignments of

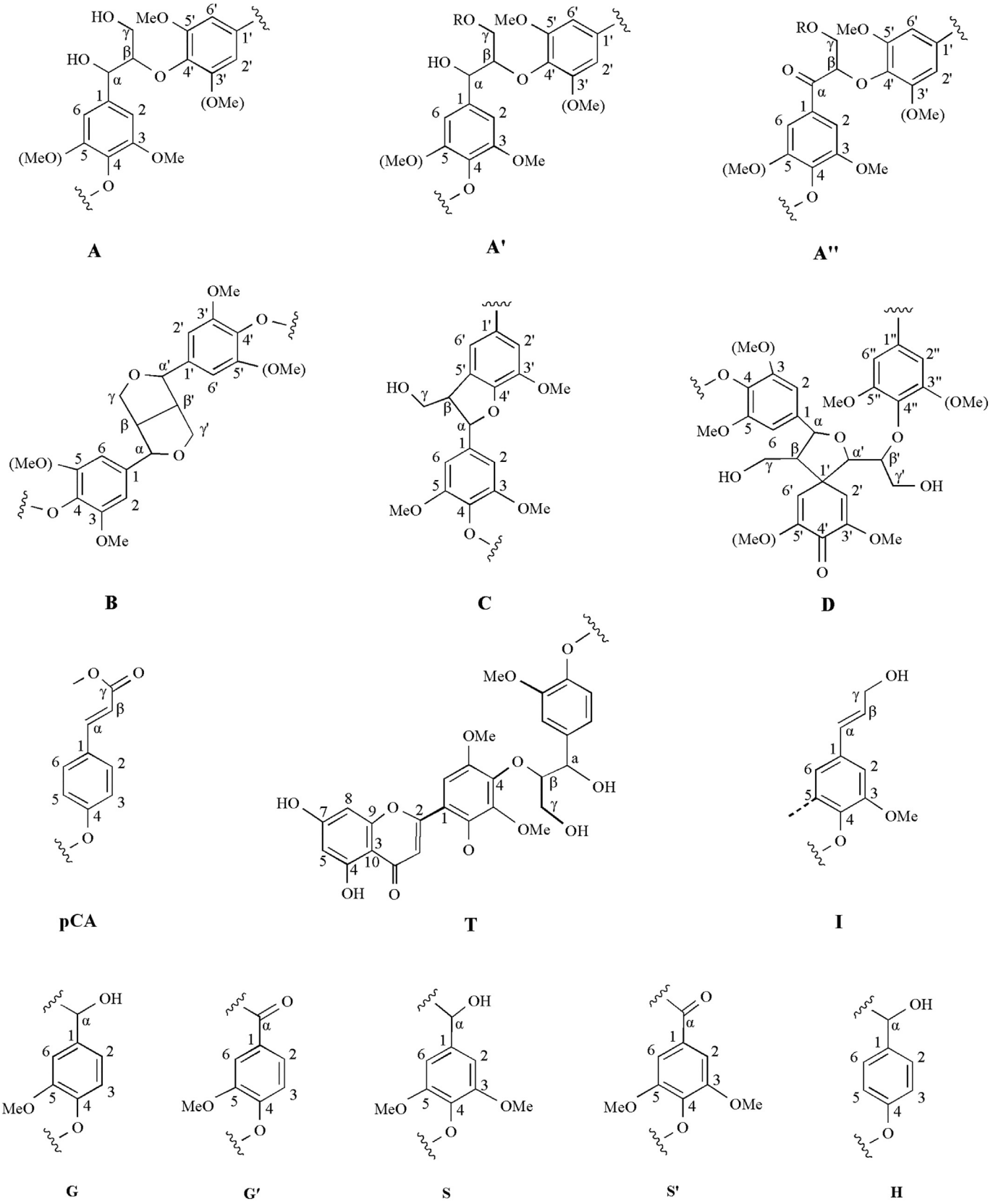

Fig. 3. Substructures presented in the lignin fractions isolated from *D. sinicus*: (A) β-*O*-4′ linkages; (A′) γ-acetylated β-*O*-4′ substructures; (A′′) γ-*p*-coumaroylated β-*O*-4′ linkages; (B) resinol structures formed by β-β′/α-*O*-γ′/γ-*O*-α′ linkages; (C) phenylcoumarane structures formed by β-5′/α-*O*-4′ linkages; (D) spirodienone structures formed by β-1′/α-*O*-α'linkages; (*p*CA) *p*-coumarate ester structures; (T) a likely incorporation of tricin into the lignin polymer through a G-type β-*O*-4′ linkage; (I) *p*-hydroxycinnamyl alcohol end groups; (G) guaiacyl unit; (G′) oxidized guaiacyl units with a C_α ketone; (S) syringyl unit; (S′) oxidized syringyl unit linked a carbonyl group at C_α (phenolic); (H) *p*-hydroxy phenylpropane unit.

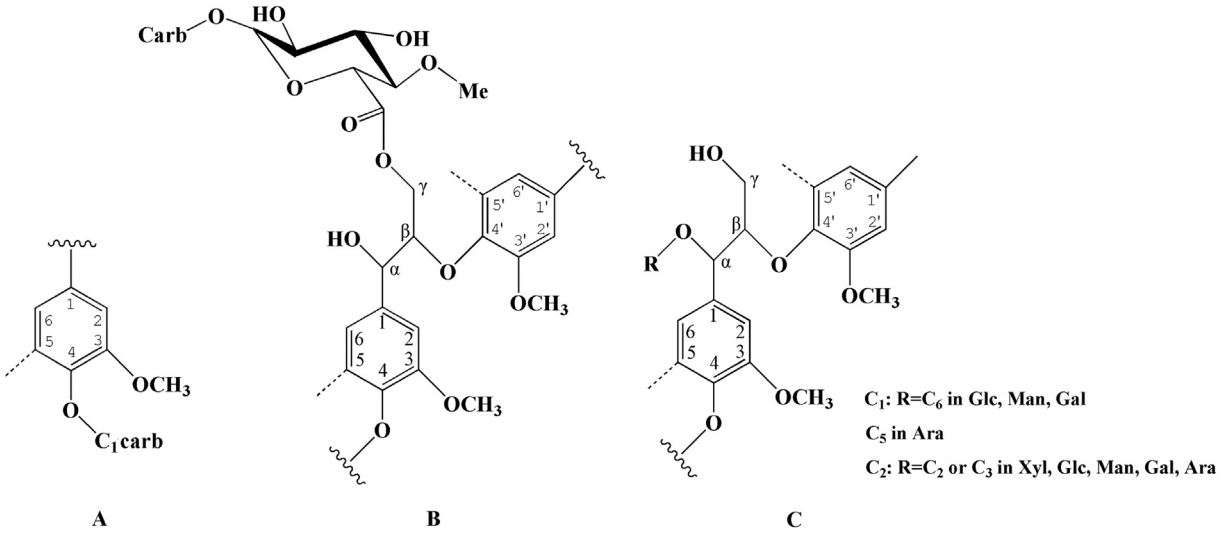

Fig. 4. Lignin-carbohydrate linkages: phenyl glycoside (A), γ-ester (B), and benzyl ether (C).

the main lignin and associated carbohydrate cross signals in the HSQC spectra are listed in Table 3.

3.4.1. Lignin structures

The side-chain region of the spectra gave important information about the different interunit linkages present in the bamboo lignin. As shown in Fig. 2, both the HSQC spectra of MWL and DSL showed prominent signals corresponding to β-*O*-4′ substructures (A). The C-H correlations in β-*O*-4′ substructures were observed for α-C positions at δ_C/δ_H 71.8/4.86 (structures A and A´), and for β-C positions of S-type lignin corresponding to *erythro* and *threo* forms at δ_C/δ_H 85.9/4.12 and 86.3/4.29, respectively. However, the correlations shifted to δ_C/δ_H 83.5/4.29 in structures A linked to G/H lignin units and γ-acylated β-*O*-4′ aryl ether substructures (A´) linked to S lignin units. The C-H correlations for γ-C positions in β-*O*-4′ substructures were observed at δ_C/δ_H 59.5/3.63 and 63.2/4.33–4.49 for structure A and A´, respectively. The presence of signals of A′ indicated that the lignin of bamboo *D. sinicus* is partially acetylated at γ-C positions in side chain of β-*O*-4′ substructures. In addition to β-*O*-4′ aryl ether structures, other various interunit linkages were also observed in significant amounts. Strong signals for resinol (β-β′/α-*O*-γ′/γ-*O*-α′) substructures (B) were observed in the spectra, with their C_α-H_α, C_β-H_β and the double C_γ-H_γ correlations at δ_C/δ_H 84.8/4.65, 53.5/3.06 and 71.4/3.82 and 4.18 ppm, respectively. The phenylcoumaran substructures (C) were detected from the spectra, and the signals for their C_α-H_α, C_β-H_β, and C_γ-H_γ correlations were observed at δ_C/δ_H 86.8/5.46, 53.3/3.46, and 62.5/3.73 ppm, respectively. In bamboo lignin MWL, very small signals corresponding to *p*-hydroxycinnamyl alcohol end groups (I) could be detected. However, this group is really rare in plant lignin, which was the main reason for the weak signals in the spectra. Furthermore, very small signals (C_α-H_α correlations at δ_C/δ_H 79.2/5.59 ppm) corresponding to spirodienone (β-1′ and α-*O*-α′) substructures (D) could be observed when HSQC-NMR spectra were Amplified (not shown in Fig. 2). However, these interunit linkages are really rare in nature, which was the main reason for the weak signals in the spectra.

The main cross-signals in the aromatic region of the HSQC spectra corresponded to the aromatic rings of the different lignin units. Signals from syringyl, guaiacyl, and *p*-hydroxyphenyl units were observed from the HSQC spectra of bamboo *D. sinicus* lignin. The syringyl lignin units showed a prominent signal for the correlation of $C_{2,6}$-$H_{2,6}$ at δ_C/δ_H 104.4/6.73 ppm, while the correlation of $C_{2,6}$-$H_{2,6}$ in oxidized syringyl unit linked a carbonyl group at C_α (phenolic) were detected at δ_C/δ_H 106.2/7.23. The guaiacyl lignin units showed different correlations for C_2-H_2 (δ_C/δ_H 110.7/6.98 ppm), C_5-H_5 (δ_C/δ_H 114.8/6.77 ppm), and C_6-H_6 (δ_C/δ_H 119.4/6.75 ppm). Meanwhile, a significant amount of *p*-hydroxyphenyl units was observed from $C_{2,6}$-$H_{2,6}$ correlations at δ_C/δ_H 127.9/7.19 ppm. In addition, it was easy to identify correlations of esterified *p*-coumaric acid structures (*p*CA) due to its very prominent signals as shown by HSQC spectra. Aromatic ring cross-signals corresponding to correlations $C_{2,6}$-$H_{2,6}$ and $C_{3,5}$-$H_{3,5}$ in *p*CA were observed at δ_C/δ_H 130.1/7.49 and 115.7/6.94 ppm, respectively. Side chain cross-signals corresponding to correlations C_α and C_β in *p*CA were revealed at 144.3/7.51 and 115.7/6.30 ppm, respectively.

Río first report that the tricin was incorporated into wheat straw lignin in 2012 [31]. Their research implied that an unrevealed biosynthetic pathway may be associated with cell wall lignification in gramineous

Table 3
Assignments of ^{13}C-^{1}H correlation signals in the HSQC spectra of lignin fractions (MWL and DSL) isolated from *D. sinicus*.

Lables	δ_C/δ_H	Assignments
C_β	53.3/3.46	C_β–H_β in phenylcoumaran substructures (C)
B_β	53.5/3.06	C_β–H_β in β-β′ (resinol) substructures (B)
MeO	55.6/3.70	C–H in methoxyls
A_γ	59.5/3.63	C_γ–H_γ in β-*O*-4′ substructures (A)
C_γ	62.5/3.73	C_γ–H_γ in phenylcoumaran substructures (C)
A'_γ	63.2/4.33–4.49	C_γ–H_γ in β-*O*-4′ substructures (A′)
B_γ	71.4/3.82, 4.18	C_γ–H_γ in β-β′ resinol substructures (B)
A_α	71.8/4.86	C_α–H_α in β-*O*-4′ substructures linked to a S unit (A, A′)
$D_{\beta'}$	79.2/4.12	$C_{\beta'}$–$H_{\beta'}$ in spirodienone substructures (D)
$A_{\beta(G/H)}$	83.5/4.29	C_β–H_β in β-*O*-4′ substructures linked to a G and H unit (A, A′)
B_α	84.8/4.65	C_α–H_α in β-β′ (resinol) substructures (B)
$A_{\beta(S)}$	85.9/4.12, 86.3/4.29	C_β–H_β in β-*O*-4′ substructures linked to a S unit (A)
C_α	86.8/5.46	C_α–H_α in phenylcoumaran substructures (C)
T_8	93.6/6.60	C_8–H_8 in tricin substructures (T)
T_6	98.2/6.22	$C_{2,6}$–$H_{2,6}$ in tricin substructures (T)
$T'_{2,6}$	103.2/7.34	$C'_{2,6}$–$H'_{2,6}$ in tricin substructures (T)
$S_{2,6}$	104.3/6.73	$C_{2,6}$–$H_{2,6}$ in etherified syringyl units (S)
$S'_{2,6}$	106.2/7.23	$C_{2,6}$–$H_{2,6}$ in oxidized (C_α = O) phenolic syringyl units (S′)
G_2	110.7/6.98	C_2–H_2 in guaiacyl units (G)
G_5	114.8/6.77	C_5–H_5 in guaiacyl units (G)
pCA_β	113.9/6.30	C_β–H_β, *p*-coumaroylated substructures (*p*CA)
$pCA_{3,5}$	115.7/6.94	$C_{3,5}$–$H_{3,5}$, *p*-coumaroylated substructures (*p*CA)
G_6	119.4/6.75	C_6–H_6, G units (G)
$H_{2,6}$	127.9/7.19	$C_{2,6}$–$H_{2,6}$ in H units (H)
$pCA_{2,6}$	130.1/7.49	$C_{2,6}$–$H_{2,6}$, *p*-coumaroylated substructures (*p*CA)
pCA_α	144.3/7.51	C_α–H_α, *p*-coumaroylated substructures (*p*CA)

Abbreviations: G, guaiacyl unit; S, syringyl unit; S′, oxidized syringyl unit linked a carbonyl group at C_α (phenolic); H, *p*-hydroxylphenyl unit; pCA, esterified *p*-coumaric acid.

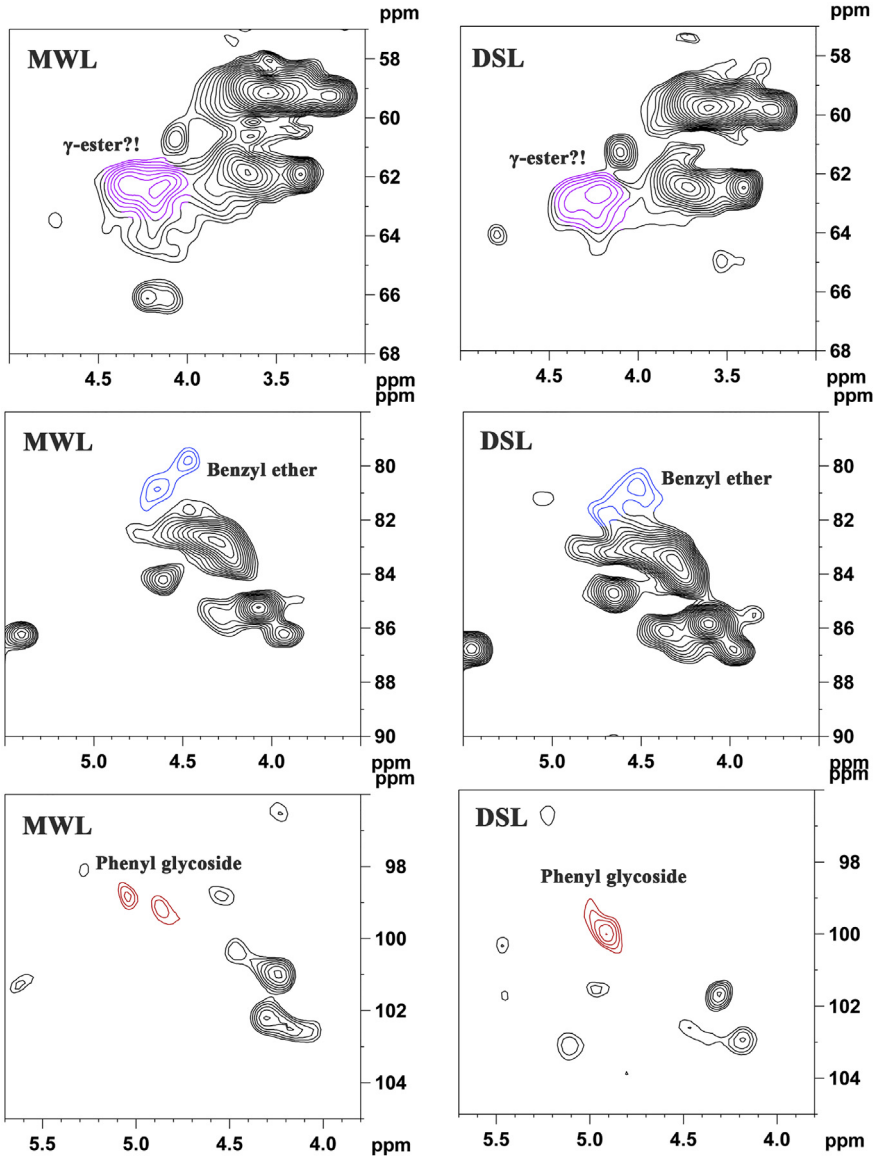

Fig. 5. Amplified anomeric regions of HSQC-NMR spectra of phenyl glycoside, γ-ester, and benzyl ether in bamboo lignin fractions (MWL, DSL) isolated from *D. sinicus*.

plants. In recent years, Wen et al. [28] and Huang et al. [32–34] sequentially reported that tricin might belong to trace substructures in milled wood lignin of Moso bamboo culm. In our present research, the signals corresponding to the tricin substructure (T) were detected in both spectra of MWL and DSL according to the C-H correlations at δ_C/δ_H 93.6/6.60, 98.2/6.22, and 103.2/7.34 [35]. However, according to our previous findings, the signals of tricin could not be detected in the bamboo lignin isolated from *D. sinicus* with NaOH solution [36]. The results imply that it was necessary to separate lignin from plant cell wall under mild and neutral conditions to ensure a native structural characteristic when the polymer's structure was evaluated.

3.4.2. LCC structures

It is generally believed that there are three types of LCC linkages in the lignocellulosic biomass, phenyl glycoside (PhGlc), benzyl ether (BE), and γ-ester. According to the NMR data from lignin-carbohydrate model compounds, PhGlc linkages can be detected in the signals area of δ_C/δ_H 104–99/4.8–5.2, and the signal of the LCC γ-ester should be observed in the signals area of δ_C/δ_H 65–62/4.0–4.5. Benzyl ether LCC structures can be subdivided into two types: (a) BE_1 linkages between the α-position of lignin and the primary OH groups of carbohydrates, which can be observed in the signals area of δ_C/δ_H 81–80/4.5–4.7 (at C-6 of Glc, Gal, and Man, and C-5 of Ara); and (b) BE_2 linkages between the α-position of lignin and secondary OH groups of carbohydrates, mainly of lignin-xylan type (at C-2 or C-3 of Xyl), giving a cross-peak at δ_C/δ_H 81–80/4.9–5.1.

In the present study, the cross signals at δ_C/δ_H 100.1/4.91 ppm was labeled as PhGlc. The C_α-H_α correlations signals at δ_C/δ_H 81.0/4.62 in the HSQC spectra of MWL and DSL implied that the BE LCC structures were BE_1 type in bamboo *D. sinicus* lignin. However, signals for γ-ester bonds were overlaps with the correlations of γ-acylated β-*O*-4′ aryl ether substructures (A′) at δ_C/δ_H 65–62/4.0–4.5 ppm. Therefore, further research was needed to confirm the exact presence of the γ-ester LCC linkages.

4. Conclusions

To characterize the structures of lignin and lignin-carbohydrate complex, two lignin fractions (MWL, DSL) were isolated with dioxane and DMSO under mild and neutral condition from the largest bamboo species in the world, *D. sinicus*. The results showed that the two-step treatments yielded 52.1% lignin based on the total lignin content in

the dewaxed bamboo sample. The bamboo lignin consisted of three basic units, *p*-hydroxyphenyl, guaiacyl, and syringyl units. The major interunit linkages presented in the obtained bamboo lignin were *β-O-4′* aryl ether linkages, together with lower amounts of *β-β′*, *β-5′*, and *β-1′* linkages. Meanwhile, tricin was detected to be linked to lignin polymer through *β-O-4′* linkage in the bamboo. In addition, phenyl glycoside and benzyl ether LCC linkages were clearly detected in bamboo (*D. sinicus*), whereas the γ-ester LCC linkages were ambiguous due to the overlapping NMR signals with other substructures. The detailed structural properties of the obtained lignin fraction together with the light-weight, as compared with the heavy weight of metals and ceramic systems [37–49], will benefit efficient utilization of natural polymers as a possibly large-scale bio-based precursor for making polymeric materials, biochemicals, functional carbon and biofuels, and multifunctional polymer nanocomposites as well to be potentially used for fuel cells, electromagnetic interference (EMI) shielding, adsorbents for environmental remediation, anticorrosion coating, sensors, etc. [50–78].

Acknowledgment

The work was financially supported by National Natural Science Foundation of China (31560195, 31760195, and 51508484), Fundamental Research Funds of Yunnan Province, China (2018FB066), Yunling Industrial Technology Leading Talent of Yunnan Province, China (2018-212, 2016HB005), and Guanxi Key Laboratory of Chemistry and Engineering of Forest Products, China (2017AD19029). Thanks were also given to Dr. Tong-qi Yuan and Jia-long Wen in Beijing Forestry University for their grateful help on the NMR analysis in the present research.

Appendix A. Supplementary data

Supplementary data to this article can be found online at https://doi.org/10.1016/j.ijbiomac.2018.12.234.

References

[1] P. Sannigrahi, A.J. Ragauskas, Characterization of fermentation residues from the production of bio-ethanol from lignocellulosic feedstocks, J. Biobased Mater. Bioenergy 5 (2011) 514–519.
[2] Z. Zheng, O. Olayinka, B. Li, 2S-Soy protein-based biopolymer as a non-covalent surfactant and its effects on electrical conduction and electric relaxation of polymer nanocomposites, Eng. Sci. 4 (2018) 87–99, https://doi.org/10.30919/es8d766.
[3] A.J. Ragauskas, G.T. Beckham, M.J. Biddy, R. Chandra, F. Chen, M.F. Davis, B.H. Davison, R.A. Dixon, P. Gilna, M. Keller, P. Langan, A.K. Naskar, J.N. Saddler, T.J. Tschaplinski, G.A. Tuskan, C.E. Wyman, Lignin valorization: improving lignin processing in the biorefinery, Science 344 (2014) 1246843.
[4] Z. Liu, X. Lu, J. Xie, B. Feng, Q. Han, Synthesis of a novel tunable lignin-based star copolymer and its flocculation performance in the treatment of kaolin suspension, Sep. Purif. Technol. 210 (2019) 355–363.
[5] L. Yang, X.F. Wang, Y. Cui, Y.M. Tian, H.Z. Chen, Z.C. Wang, Modification of renewable resources-lignin-by three chemical methods and its applications to polyurethane foams, Polym. Adv. Technol. 25 (2014) 1089–1098.
[6] D. Ohrnberger, Subfamily Bambusoideae, in: D. Ohrnberger (Ed.), The Bamboos of the World, Elsevier, Amsterdam 1999, pp. 7–29.
[7] F.X. Yue, F.C. Lu, M. Regner, R.C. Sun, J. Ralph, Lignin-derived thioacidolysis dimers: reevaluation, new products, authentication, and quantification, ChemSusChem 10 (2017) 830–835.
[8] M. Balakshin, E. Capanema, A. Berlin, Chapter 4-isolation and analysis of lignin-carbohydrate complexes preparations with traditional and advanced methods: A review, in: R. Atta (Ed.), Studies in Natural Products Chemistry, Elsevier 2014, pp. 83–115.
[9] M. Lawoko, G. Henriksson, G. Gellerstedt, Structural differences between the lignin-carbohydrate complexes present in wood and in chemical pulps, Biomacromolecules 6 (2005) 3467–3473.
[10] J.J. Zeng, G.L. Helms, X. Gao, S.L. Chen, Quantification of wheat straw lignin structure by comprehensive NMR analysis, J. Agric. Food Chem. 61 (2013) 10848–10857.
[11] Y.Z. Lai, K.V. Sarkanen, Isolation and structural studies, in: K.V. Sarkanen, C.H. Ludwig (Eds.), Lignins, Occurrence, Formation, Structure and Reactions, Wiley-Interscience, New York 1971, pp. 165–240.
[12] M. Balakshin, E. Capanema, H. Gracz, Chang H-m, H. Jameel, Quantification of lignin–carbohydrate linkages with high-resolution NMR spectroscopy, Planta 233 (2011) 1097–1110.
[13] F. Zikeli, T. Ters, K. Fackler, E. Srebotnik, J. Li, Wheat straw lignin fractionation and characterization as lignin-carbohydrate complexes, Ind. Crop. Prod. 85 (2016) 309–317.
[14] A. Sluiter, R. Ruiz, C. Scarlata, J. Sluiter, D. Templeton, D. Crocker, Determination of Structural Carbohydrates and Lignin in Biomass, National Renewable Energy Laboratory, USA, 2008.
[15] A. Björkman, Isolation of lignin from finely divided wood with neutral solvents, Nature 174 (1954) 1057–1058.
[16] R.C. Sun, J.M. Fang, J. Tomkinson, Fractional isolation and structural characterization of lignins from oil palm trunk and empty fruit bunch fibers, J. Wood Chem. Technol. 19 (1999) 335–356.
[17] F. Xu, J.X. Jiang, R.C. Sun, J.N. Tang, J.X. Sun, Y.Q. Su, Fractional isolation and structural characterization of mild ball-milled lignin in high yield and purity from *Eucommia ulmoides* Oliv, Wood Sci. Technol. 42 (2008) 211–226.
[18] Z.J. Shi, L.P. Xiao, J. Deng, F. Xu, R.C. Sun, Physicochemical characterization of lignin fractions sequentially isolated from bamboo (*Dendrocalamus brandisii*) with hot water and alkaline ethanol solution, J. Appl. Polym. Sci. 125 (2012) 3290–3301.
[19] F. Xu, J.X. Sun, Z.C. Geng, C.F. Liu, J.L. Ren, R.C. Sun, P. Fowler, M.S. Baird, Comparative study of water-soluble and alkali-soluble hemicelluloses from perennial ryegrass leaves (*Lolium peree*), Carbohydr. Polym. 67 (2007) 56–65.
[20] A.S. Jääskeläinen, Y. Sun, D.S. Argyropoulos, T. Tamminen, B. Hortling, The effect of isolation method on the chemical structure of residual lignin, Wood Sci. Technol. 37 (2003) 91–102.
[21] A.V. Marques, H. Pereira, J. Rodrigues, D. Meier, O. Faix, Isolation and comparative characterization of a Björkman lignin from the saponified cork of Douglas-fir bark, J. Anal. Appl. Pyrolysis 77 (2006) 169–176.
[22] O. Faix, Classification of lignins from different botanical origins by FT-IR spectroscopy, Holzforschung 45 (1991) 21–28.
[23] J. Pinho, J. Canário, R. Cesário, C. Vale, A rapid acid digestion method with ICP-MS detection for the determination of selenium in dry sediments, Anal. Chim. Acta 551 (2005) 207–212.
[24] D. Fengel, X. Shao, Studies on the lignin of the bamboo species *Phyllostachys makinoi* Hay, Wood Sci. Technol. 19 (1985) 131–137.
[25] J.L. Wen, B.L. Xue, F. Xu, R.C. Sun, A. Pinkert, Unmasking the structural features and property of lignin from bamboo, Ind. Crop. Prod. 42 (2013) 332–343.
[26] X.Y. Du, M. Pérez-Boada, C. Fernández, J. Rencoret, J.C. del Río, J. Jiménez-Barbero, J. Li, A. Gutiérrez, A.T. Martínez, Analysis of lignin–carbohydrate and lignin–lignin linkages after hydrolase treatment of xylan–lignin, glucomannan-lignin and glucan-lignin complexes from spruce wood, Planta 239 (2014) 1079–1090.
[27] S.D. Mansfield, H. Kim, F. Lu, J. Ralph, Whole plant cell wall characterization using solution-state 2D NMR, Nat. Protoc. 7 (2012) 1579–1589.
[28] J.L. Wen, S.L. Sun, B.L. Xue, R.C. Sun, Quantitative structural characterization of the lignins from the stem and pith of bamboo (*Phyllostachys pubescens*), Holzforschung 67 (2013) 613–627.
[29] M. Li, C. Foster, S. Kelkar, Y. Pu, D. Holmes, A. Ragauskas, C.M. Saffron, D.B. Hodge, Structural characterization of alkaline hydrogen peroxide pretreated grasses exhibiting diverse lignin phenotypes, Biotechnol. Biofuels 5 (2012) 38.
[30] C. Crestini, H. Lange, M. Sette, D.S. Argyropoulos, On the structure of softwood kraft lignin, Green Chem. 19 (2017) 4104–4121.
[31] J.C. del Río, J. Rencoret, P. Prinsen, Á.T. Martínez, J. Ralph, A. Gutiérrez, Structural characterization of wheat straw lignin as revealed by analytical pyrolysis, 2D-NMR, and reductive cleavage methods, J. Agric. Food Chem. 60 (2012) 5922–5935.
[32] C.X. Huang, S. Tang, W.Y. Zhang, Y.H. Tao, C.H. Lai, Q. Yong, Unveiling the structural properties of lignin-carbohydrate complexes in bamboo residues and its functionality as antioxidants and immunostimulants, ACS Sustain. Chem. Eng. (2018)https://doi.org/10.1021/acssuschemeng.8b03262.
[33] C.X. Huang, J. He, X. Li, D.Y. Min, Q. Yong, Facilitating the enzymatic saccharification of pulped bamboo residues by degrading the remained xylan and lignin–carbohydrates complexes, Bioresour. Technol. 192 (2015) 471–477.
[34] C.X. Huang, J. He, L.T. Du, D.Y. Min, Q. Yong, Structural characterization of the lignins from the green and yellow bamboo of bamboo culm (*Phyllostachys pubescens*), J. Wood Chem. Technol. 36 (2016) 157–172.
[35] M. Li, Y.Q. Pu, T.J. Tschaplinski, A.J. Ragauskas, ^{31}P NMR characterization of tricin and its structurally similar flavonoids, Chem. Select 2 (2017) 3557–3561.
[36] Z.J. Shi, L.P. Xiao, J. Deng, R.C. Sun, Isolation and structural characterization of lignin polymer from *Dendrocalamus sinicus*, BioEnergy Res. 6 (2013) 1212–1222.
[37] Z. Zhao, R. Guan, J. Zhang, Z. Zhao, P. Bai, Effects of process parameters of semisolid stirring on microstructure of $Mg_{-3}Sn_{-1}Mn_{-3}SiC$ (wt%) strip processed by rheo-rolling, Acta Metall. Sin. (Eng. Lett.) 30 (2017) 66–72.
[38] Z. Zhao, P. Bail, R. Guan, V. Murugadoss, H. Liu, X. Wang, Z. Guo, Microstructural evolution and mechanical strengthening mechanism of $Mg_{-3}Sn_{-1}Mn_{-1}La$ alloy after heat treatments, Mater. Sci. Eng. A 734 (2018) 200–209.
[39] Z. Zhao, R. Misra, P. Bai, J. Gao, Y. Li, R. Guan, Z. Guo, Novel process of coating Al on graphene involving organic aluminum accompanying microstructure evolution, Mater. Lett. 232 (2018) 202–205.
[40] Y. Zhao, L. Qi, Y. Jin, K. Wang, J. Tian, P. Han, The structural, elastic, electronic properties and Debye temperature of D022-Ni3V under pressure from first-principles, J. Alloys Compd. 647 (2015) 1104–1110.
[41] Y. Zhao, B. Zhang, H. Hou, W. Chen, M. Wang, Phase-field simulation for the evolution of solid/liquid interface front in directional solidification process, J. Mater. Sci. Technol. (2019)https://doi.org/10.1016/j.jmst.2018.12.009.
[42] Y. Zhao, S. Deng, H. Liu, J. Zhang, Z. Guo, H. Hou, First-principle investigation of pressure and temperature influence on structural, mechanical and thermodynamic properties of Ti_3AC_2 (A = Al and Si), Comput. Mater. Sci. 154 (2018) 365–370.
[43] Y. Zhao, X. Tian, B. Zhao, Y. Sun, H. Guo, M. Dong, H. Liu, X. Wang, Z. Guo, A. Umar, H. Hou, Precipitation sequence of middle Al concentration alloy using the inversion algorithm and microscopic phase field model, Sci. Adv. Mater. 10 (2018) 1793–1804.
[44] B. Kirubasankar, V. Murugadoss, J. Lin, T. Ding, M. Dong, H. Liu, J. Zhang, T. Li, N. Wang, Z. Guo, S. Angaiaha, In-situ grown nickel selenide onto graphene nanohybrid

electrodes for high energy density asymmetric supercapacitors, Nanoscale 10 (2018) 20414–20425.
[45] W. Zhao, X. Li, R. Yin, L. Qian, X. Huang, H. Liu, J. Zhang, J. Wang, T. Ding, Z. Guo, Urchin-like NiO-$NiCo_2O_4$ heterostructure microsphere catalysts for enhanced rechargeable non-aqueous Li-O_2 batteries, Nanoscale 11 (2019) 50–59.
[46] W. Du, X. Wang, J. Zhan, X. Sun, L. Kang, F. Jiang, X. Zhang, Q. Shao, M. Dong, H. Liu, V. Murugadoss, Z. Guo, Biological cell template synthesis of nitrogen-doped porous hollow carbon spheres/MnO_2 composites for high-performance asymmetric supercapacitors, Electrochim. Acta 296 (2019) 907–915.
[47] M. Idrees, S. Batool, J. Kong, Q. Zhuang, H. Liu, Q. Shao, N. Lu, Y. Feng, E.K. Wujcik, Q. Gao, T. Ding, R. Wei, Z. Guo, Polyborosilazane derived ceramics - nitrogen sulfur dual doped graphene nanocomposite anode for enhanced lithium ion batteries, Electrochim. Acta 296 (2019) 925–937.
[48] Y. Sheng, J. Yang, F. Wang, L. Liu, H. Liu, C. Yan, Z. Guo, Sol-gel synthesized hexagonal boron nitride/titania nanocomposites with enhanced photocatalytic activity, Appl. Surf. Sci. 465 (2019) 154–163.
[49] H. Du, Y. An, X. Zhang, Y. Wei, L. Hou, B. Liu, H. Liu, J. Zhang, N. Wang, A. Umar, Z. Guo, Hydroxyapatite (HA) modified nanocoating enhancement on AZ31 Mg alloy by combined surface mechanical attrition treatment and electrochemical deposition approach, J. Nanosci. Nanotechnol. 19 (2019) 810–818.
[50] Z. Qu, M. Shi, H. Wu, Y. Liu, J. Jiang, C. Yan, An efficient binder-free electrode with multiple carbonized channels wrapped by $NiCo_2O_4$ nanosheets for high-performance capacitive energy storage, J. Power Sources 410-411 (2019) 179–187.
[51] Z. Wang, H. Zhu, N. Cao, R. Du, Y. Liu, G. Zhao, Superhydrophobic surfaces with excellent abrasion resistance based on benzoxazine/mesoporous SiO_2, Mater. Lett. 186 (2017) 274–278.
[52] D. Jiang, V. Murugadoss, Y. Wang, J. Lin, T. Ding, Z. Wang, Q. Shao, C. Wang, H. Liu, N. Lu, R. Wei, S. Angaiah, Z. Guo, Electromagnetic interference shielding polymers and nanocomposites – a review, Polym. Rev. (2018)https://doi.org/10.1080/15583724.2018.1546737 (in press).
[53] C. Wang, B. Mo, Z. He, C.X. Zhao, L. Zhang, Q. Shao, X. Guo, E. Wujcik, Z. Guo, Hydroxide ions transportation in polynorbornene anion exchange membrane, Polymer 138 (2018) 363–368.
[54] C. Wang, B. Mo, Z. He, Q. Shao, D. Pan, E. Wujick, J. Guo, X. Xie, X. Xie, Z. Guo, Crosslinked norbornene copolymer anion exchange membrane for fuel cells, J. Membr. Sci. 556 (2018) 118–125.
[55] M. Dong, Q. Li, H. Liu, C. Liu, E. Wujcik, Q. Shao, T. Ding, X. Mai, C. Shen, Z. Guo, Thermoplastic polyurethane-carbon black nanocomposite coating: fabrication and solid particle erosion resistance, Polymer 158 (2018) 381–390.
[56] Z. Wang, R. Wei, J. Gu, H. Liu, C. Liu, C. Luo, J. Kong, Q. Shao, N. Wang, Z. Guo, X. Liu, Ultralight, highly compressible and fire-retardant graphene aerogel with self-adjustable electromagnetic wave absorption, Carbon 139 (2018) 1126–1135.
[57] C. Wang, V. Murugadoss, J. Kong, Z. He, X. Mai, Q. Shao, Y. Chen, L. Guo, C. Liu, S. Angaiah, Z. Guo, Overview of carbon nanostructures and nanocomposites for electromagnetic wave shielding, Carbon 140 (2018) 696–733.
[58] L. Wang, H. Qiu, C. Liang, P. Song, Y. Han, Y. Han, J. Gu, J. Kong, D. Pan, Z. Guo, Electromagnetic interference shielding MWCNT-Fe_3O_4@Ag/epoxy nanocomposites with satisfactory thermal conductivity and high thermal stability, Carbon 141 (2019) 506–514.
[59] H. Gu, H. Zhang, C. Ma, X. Xu, Y. Wang, Z. Wang, R. Wei, H. Liu, C. Liu, Q. Shao, X. Mai, Z. Guo, Trace electrosprayed nanopolystyrene facilitated dispersion of multiwalled carbon nanotubes: simultaneously strengthening and toughening epoxy, Carbon 142 (2019) 131–140.
[60] N. Wu, C. Liu, D. Xu, J. Liu, W. Liu, Q. Shao, Z. Guo, Enhanced electromagnetic wave absorption of three-dimensional porous Fe_3O_4/C composite flowers, ACS Sustain. Chem. Eng. 6 (2018) 12471–12480.
[61] Y. Kong, Y. Li, G. Hu, J. Lin, D. Pan, D. Dong, E. Wujick, Q. Shao, M. Wu, J. Zhao, Z. Guo, Preparation of polystyrene-b-poly(ethylene/propylene)-b-polystyrene grafted glycidyl methacrylate and its compatibility with recycled polypropylene/recycled high impact polystyrene blends, Polymer 145 (2018) 232–241.
[62] Y. Ma, L. Lyu, Y. Guo, Y. Fu, Q. Shao, T. Wu, S. Guo, K. Sun, X. Guo, E.K. Wujcik, Z. Guo, Porous lignin based poly (acrylic acid)/organo-montmorillonite nanocomposites: swelling behaviors and rapid removal of Pb (II) ions, Polymer 128 (2017) 12–23.
[63] K. Gong, Q. Hu, L. Yao, M. Li, D. Sun, Q. Shao, B. Qiu, Z. Guo, Ultrasonic pretreated sludge derived stable magnetic active carbon for Cr(VI) removal from wastewater, ACS Sustain. Chem. Eng. 6 (2018) 7283–7291.
[64] Y. Wang, P. Zhou, S. Luo, X. Liao, B. Wang, Q. Shao, X. Guo, Z. Guo, Controllable synthesis of monolayer poly(acrylic acid) on channel surface of mesoporous alumina for Pb(II) adsorption, Langmuir 34 (2018) 7859–7868.
[65] Z. Li, B. Wang, X. Qin, Y. Wang, C. Liu, Q. Shao, N. Wang, J. Zhang, Z. Wang, C. Shen, Z. Guo, Superhydrophobic/superoleophilic polycarbonate/carbon nanotubes porous monolith for selective oil adsorption from water, ACS Sustain. Chem. Eng. 6 (2018) 13747–13755.
[66] Z. Hu, D. Zhang, F. Lu, W. Yuan, X. Xu, Q. Zhang, H. Liu, Q. Shao, Z. Guo, Y. Huang, Multistimuli-responsive intrinsic self-healing epoxy resin constructed by host−guest interactions, Macromolecules 51 (2018) 5294–5303.
[67] H. Gu, H. Zhang, J. Lin, Q. Shao, D.P. Young, L. Sun, T.D. Shen, Z. Guo, Large negative giant magnetoresistance at room temperature and electrical transport in cobalt ferrite-polyaniline nanocomposites, Polymer 143 (2018) 324–330.
[68] H. Zhang, S. Lyu, X. Zhou, H. Gu, C. Ma, C. Wang, T. Ding, Q. Shao, H. Liu, Z. Guo, Super light 3D hierarchical nanocellulose aerogel foam with superior oil adsorption, J. Colloid Interface Sci. 536 (2019) 245–251.
[69] W. Wang, X. Hao, S. Chen, Z. Yang, C. Wang, R. Yan, X. Zhang, H. Liu, Q. Shao, Z. Guo, pH-responsive capsaicin@chitosan nanocapsules for antibiofouling in marine applications, Polymer 158 (2018) 223–230.
[70] Y. Qian, Y. Yuan, H. Wang, H. Liu, J. Zhang, S. Shi, Z. Guo, N. Wang, Highly efficient uranium adsorption by salicylaldoxime/polydopamine graphene oxide nanocomposites, J. Mater. Chem. A 6 (2018) 24676–24685.
[71] C. Wang, Z. He, X. Xie, X. Mai, Y. Li, T. Li, M. Zhao, C. Yan, H. Liu, E. Wujcik, Z. Guo, Controllable cross-linking anion exchange membranes with excellent mechanical and thermal properties, Macromol. Mater. Eng. (3) (2018), 1700462. .
[72] H. Wei, H. Wang, Y. Xia, D. Cui, Y. Shi, M. Dong, C. Liu, T. Ding, J. Zhang, Y. Ma, N. Wang, Z. Wang, Y. Sun, R. Wei, Z. Guo, An overview of lead-free piezoelectric materials and devices, J. Mater. Chem. C 6 (2018) 12446–12467.
[73] Z. Wu, H. Cui, L. Chen, D. Jiang, L. Weng, Y. Ma, X. Li, X. Zhang, H. Liu, N. Wang, J. Zhang, Y. Ma, M. Zhang, Y. Huang, Z. Guo, Interfacially reinforced unsaturated polyester carbon fiber composites with a vinyl ester-carbon nanotubes sizing agent, Compos. Sci. Technol. 164 (2018) 195–203.
[74] H. Liu, Q. Li, S. Zhang, R. Yin, X. Liu, Y. He, K. Dai, C. Shan, J. Guo, C. Liu, C. Shen, X. Wang, N. Wang, Z. Wang, R. Wei, Z. Guo, Electrically conductive polymer composites for smart flexible strain sensor: a critical review, J. Mater. Chem. C 6 (2018) 12121–12141.
[75] B. Song, T. Wang, L. Wang, H. Liu, X. Mai, X. Wang, N. Wang, Y. Huang, Y. Ma, Y. Lu, E.K. Wujcik, Z. Guo, Interfacially reinforced carbon fiber/epoxy composite laminates via in-situ synthesized graphitic carbon nitride (g-C_3N_4), Compos. Part B 158 (2019) 259–268.
[76] A. Nautiyal, M. Qiao, T. Ren, T. Huang, X. Zhang, J. Cook, M.J. Bozack, R. Farag, High-performance engineered conducting polymer film towards antimicrobial/anticorrosion applications, Eng. Sci. 4 (2018) 70–78, https://doi.org/10.30919/es8d776.
[77] Z. Hu, Q. Shao, Y. Huang, L. Yu, D. Zhang, X. Xu, J. Lin, H. Liu, Z. Guo, Light triggered interfacial damage self-healing of poly(*p*-phenylene benzobisoxazole) fiber composites, Nanotechnology 29 (2018), 185602. .
[78] K. Sun, R. Fan, X. Zhang, Z. Zhang, Z. Shi, N. Wang, P. Xie, Z. Wang, G. Fan, H. Liu, C. Liu, T. Li, C. Yan, Z. Guo, An overview of metamaterials and their achievements in wireless power transfer, J. Mater. Chem. C 6 (2018) 2925–2943.